Stem Cell Reports, Volume *18*

Supplemental Information

A defined roadmap of radial glia and astrocyte differentiation from human pluripotent stem cells

Vukasin M. Jovanovic, Claire Weber, Jaroslav Slamecka, Seungmi Ryu, Pei-Hsuan Chu, Chaitali Sen, Jason Inman, Juliana Ferreira De Sousa, Elena Barnaeva, Marissa Hirst, David Galbraith, Pinar Ormanoglu, Yogita Jethmalani, Jennifer Colon Mercado, Sam Michael, Michael E. Ward, Anton Simeonov, Ty C. Voss, Carlos A. Tristan, and Ilyas Singeç

Supplemental Information (Jovanovic et al.)

Figure S1

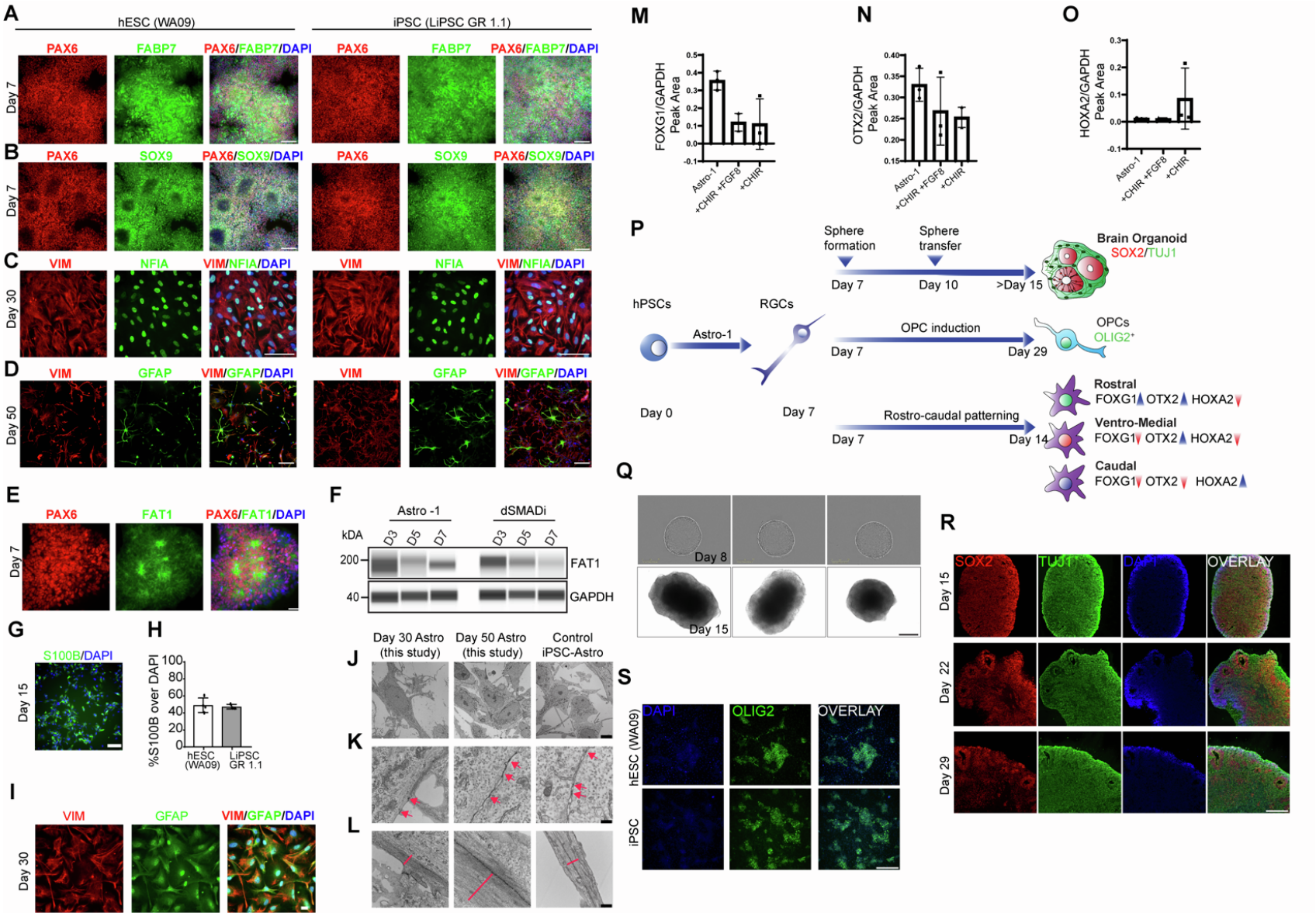

Figure S1. Reproducible generation and specification of multipotent RGCs

(A, B) Neural rosettes expressing PAX6, FABP7, and SOX9 after hPSCs (WA09 and LiPSC-GR1.1) were treated with Astro-1 medium for 7 days.

(C) Representative images showing nuclear NFIA expression in the majority of cells (day 30).

(D) Astrocytes expressing GFAP and VIM (day 50). Scale bars, 100 μm.

(E) Immunostaining showing FAT1 expression by neural rosettes.

(F) Western blot showing differences in FAT1 expression during neural induction with Astro-1 versus dSMADi.

(G) Immunocytochemistry for S100B in differentiating cultures (day 15).

(H) Quantification of S100B$^+$ cells (day 15). Data expressed as mean ± SD. n = 4 replicate wells for 2 independent cell lines (WA09, LiPSC GR 1.1).

(I) Diffuse immunoreactivity for GFAP in immature astrocytes (day 30).

(J) Electron microscopy showing typical stellate morphology of astrocytes (LiPSC-GR1.1).

(K) Astrocytes showing prominent tight junctions (red arrowheads).

(L) Astrocytic processes (red dashed lines) with abundant intermediate filaments.

(M-O) Quantitative immunoblotting after rostro-caudal patterning of RGCs demonstrating (M) downregulation of FOXG1 in response to WNT pathway activation and FGF8 administration, or WNT activation alone, (N) reduction of OTX2 expression and (O) Upregulation of HOXA2 in response to WNT activation. Each bar graph represents replicates from WA09, LiPSC GR1.1, and NCRM5.

(P) Experimental design for RGC patterning. RGCs were used to generate spheroids based on a previously published protocol (Marton et al., 2019), patterned in monolayer cultures by including SAG21K, EGF/FGF2 and RA to Astro-1 medium to generate OLIG2$^+$ progenitors, or WNT activation (CHIR99021) with and without FGF8 for caudalization (see Experimental Procedures).

(Q) Phase contrast images of RGC-derived spheroids at day 8 (24 h after spheroid formation) and day 15 (WA09).

(R) Immunohistochemistry of sectioned spheroids (day 15, 22, 29) showing neural tube-like structures with SOX2$^+$ cells surrounded by TUJ1$^+$ neurons. Note the time-dependent decrease of SOX2$^+$ cells. Scale bars 100 μm.

(S) Immunocytochemistry showing OLIG2 expression in RGCs after treatment with EGF/FGF2/SAG21k/RA over the course of 21 days. Experiments were independently reproduced with WA09 and LiPSC GR 1.1 lines. Scale bars, (A-E, I) 100 μm, (J) 10 μm, (K, L) 0.5 μm, (Q) 300 μm, (S) 100 μm.

Figure S2

A

Treatment condition	Day 0 - 7	Day 7 - 14	Day 14 -21	Sample Collection
1	BMPi	BMPi	Astro-2	Day 21
2	dSMADi	EGF/FGF	EGF/FGF	Day 21
3	Astro-1	Astro-1	Astro-2	Day 21
4	Astro-1 + FGF/EGF	Astro-1 + FGF/EGF	Astro-2 + EGF/FGF	Day 21
5	Astro-1	Astro-1	Astro-2 + EGFi/FGFi (PD17/Afatinib)	Day 21
6	Astro-1 - NOTCH	Astro-1 - NOTCH	Astro-2 - NOTCH (Jagged-1/DLL-1)	Day 21

B

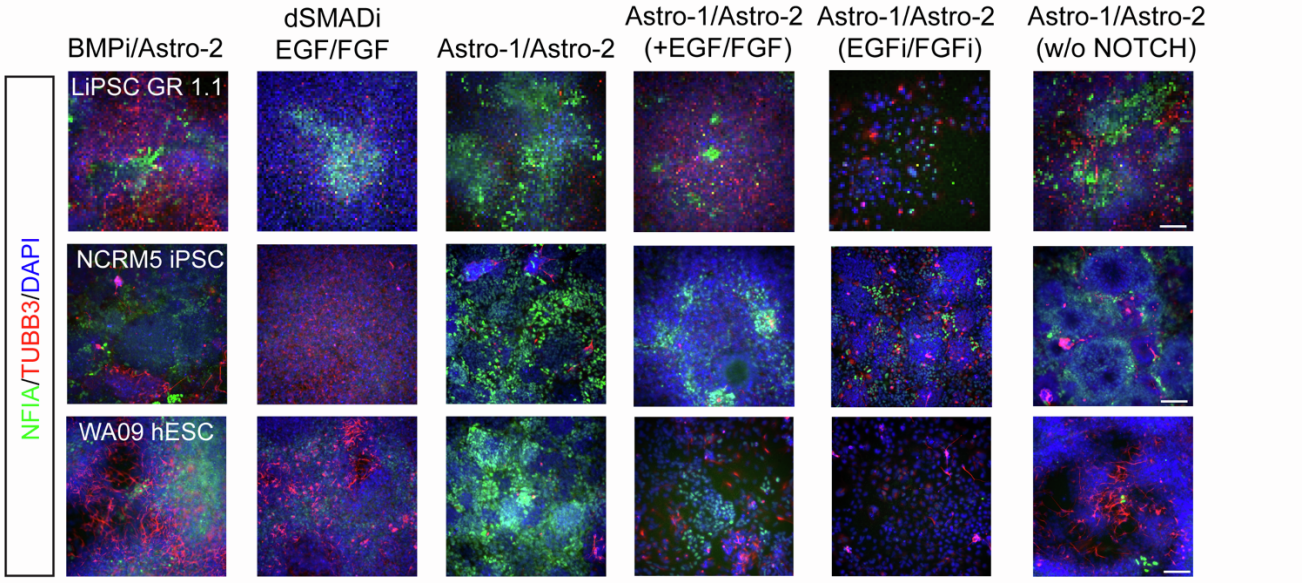

C

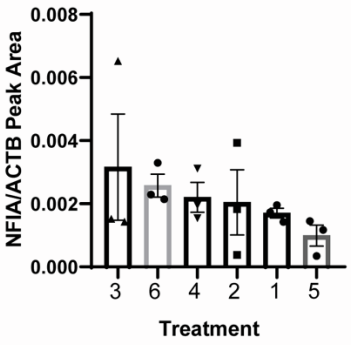

D

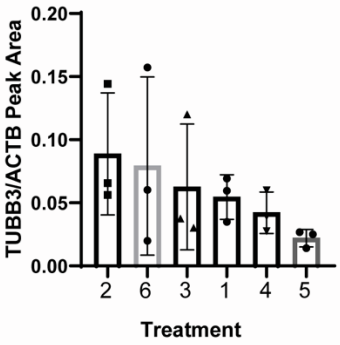

E

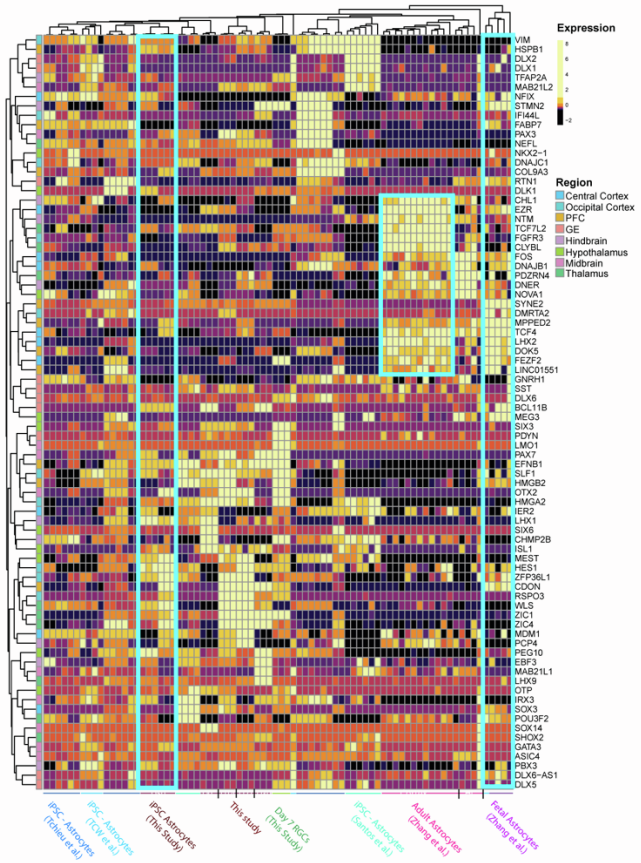

Figure S2. Characterization of Astro-1/Astro-2 media for NFIA induction and regional identity of RGCs and astrocytes.

(A) Table summarizing the treatment combinations tested over the course of 21 days. For more details see Experimental Procedures.

(B) Immunocytochemistry showing NFIA and TUBB3 expression (day 21) after differentiating 3 different cell lines (WA09, LiPSC GR 1.1, NCRM5) subjected to 6 different treatment conditions.

(C-D) Quantitative immunoblotting of NFIA and TUBB3 expression. Note the strongest average expression of NFIA with Astro-1/Astro 2 (treatment #3), and the strongest TUBB3 expression in cultures treated with dSMADi followed by cell expansion with EGF/FGF2 (treatment group #2). Experimental design and treatment groups shown in (A).

(E) Heatmap of clustering analysis for regional gene markers across samples of iPSC-derived RGCs and astrocytes from this study as well as previously published studies and comparison to primary human adult astrocytes (cortex and hippocampus) and primary human fetal astrocytes (cortex). Note the lack of regional identity in fetal astrocytes and iPSC-derived astrocytes as compared to adult human astrocytes.

Scale bars (B) 100 μm.

Figure S3

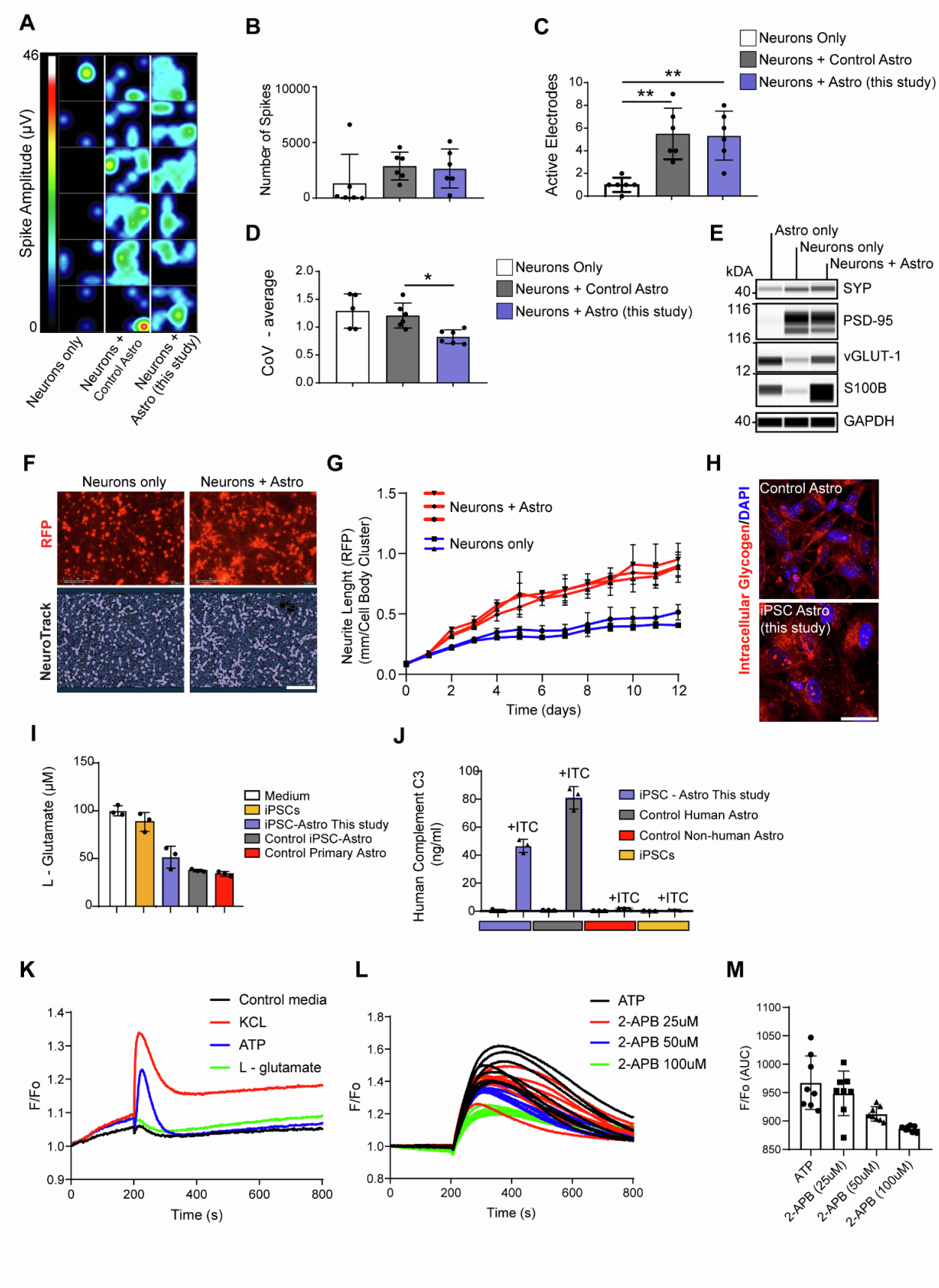
A
Spike Amplitude (µV)
46
0
Neurons only
Neurons + Control Astro
Neurons + Astro (this study)
B
Number of Spikes
10000
5000
0
C
Active Electrodes
Neurons Only
Neurons + Control Astro
Neurons + Astro (this study)
**
**
D
CoV - average
*
Neurons Only
Neurons + Control Astro
Neurons + Astro (this study)
E
Astro only
Neurons only
Neurons + Astro
kDA
SYP
PSD-95
vGLUT-1
S100B
GAPDH
F
Neurons only
Neurons + Astro
RFP
NeuroTrack
G
Neurite Lenght (RFP) (mm/Cell Body Cluster)
Neurons + Astro
Neurons only
Time (days)
H
Intracellular Glycogen/DAPI
Control Astro
iPSC Astro (this study)
I
L - Glutamate (µM)
Medium
iPSCs
iPSC-Astro This study
Control iPSC-Astro
Control Primary Astro
J
Human Complement C3 (ng/ml)
+ITC
+ITC
+ITC
+ITC
iPSC - Astro This study
Control Human Astro
Control Non-human Astro
iPSCs
K
F/Fo
Control media
KCL
ATP
L - glutamate
Time (s)
L
F/Fo
ATP
2-APB 25uM
2-APB 50uM
2-APB 100uM
Time (s)
M
F/Fo (AUC)
ATP
2-APB (25uM)
2-APB (50uM)
2-APB (100uM)

Figure S3. Functional characterization of hPSC-derived astrocytes

(A) MEA analysis showing enhanced electrical activity of glutamatergic neurons co-cultured with hPSC-astrocytes for 8 days.

(B-D) Quantification of spikes (B), active electrodes (C) and reduced coefficient of variation (D) in co-cultures as compared to neuron-only cultures. n = 6 replicate wells per experimental condition. Glutamatergic neurons and control astrocytes (FUJIFILM CDI), iPSC-astrocytes derived with the current method (LiPSC GR 1.1).

(E) Western blot analysis of neuronal markers synaptophysin (SYP), PSD-95, vesicular glutamate transporter-1 (vGLUT1), and the astrocyte marker S100B in co-cultures (21 day). Note the stronger expression of SYN and S100B in co-cultures suggesting improved differentiation of both cell types.

(F) Representative images of RFP^+ i3-neurons and image mask of cell bodies and neurites analyzed with NeuroTrack software. Co-cultured astrocytes and i3-neurons derived from the same iPSC line (WTC11).

(G) Time-course live-cell imaging and quantification of RFP^+ neurite length in neuron-only versus neuron-astrocyte co-cultures. Note the difference from day 2 onward. i3-neurons were co-cultured with astrocytes in a 1:3 ratio. Images were obtained with the IncuCyte S3 live imaging system (each data point on the graph represents a replicate well; for each well 4 images were taken and analyzed over the course of 12 days; n = 3 replicate wells for co-cultures, n = 2 replicate wells for mono-cultures).

(H) PAS stain showing intracellular glycogen in hPSC-astrocytes (LiPSC-GR1.1) and controls (iCell Astrocytes from FUJIFILM CDI). Scale bar, 100 μm

(I) Glutamate uptake by iPSC-astrocytes (NCRM5) is comparable to controls (FUJIFILM CDI) and primary mouse astrocytes (ScienCell). n = 3 replicate wells.

(J) Human complement C3 secretion by iPSC-astrocytes (NCRM5) and controls into the culture medium after stimulation with inflammatory cytokines (IL-1b, TNF-alpha and C1q) for 24 h. n = 3 replicate wells.

(K) Calcium transients in iPSC-astrocyte cultures (LiPSC-GR1.1) after stimulation with KCL, ATP and L-glutamate. Each dotted line in the graph represents average from n = 6 replicate wells.

(L) Calcium transients in iPSC-astrocyte cultures (LiPSC-GR1.1) after stimulation with ATP, pretreated for 1h with DMSO (black lines) or IP3R antagonist 2-APB in dose response manner (25, 50 and 100 μM). Each dotted line in the graph represents one well.

(M) Quantification of the area under the curve (AUC) showing reduced calcium response after 2-APB pretreatment.

Figure S4

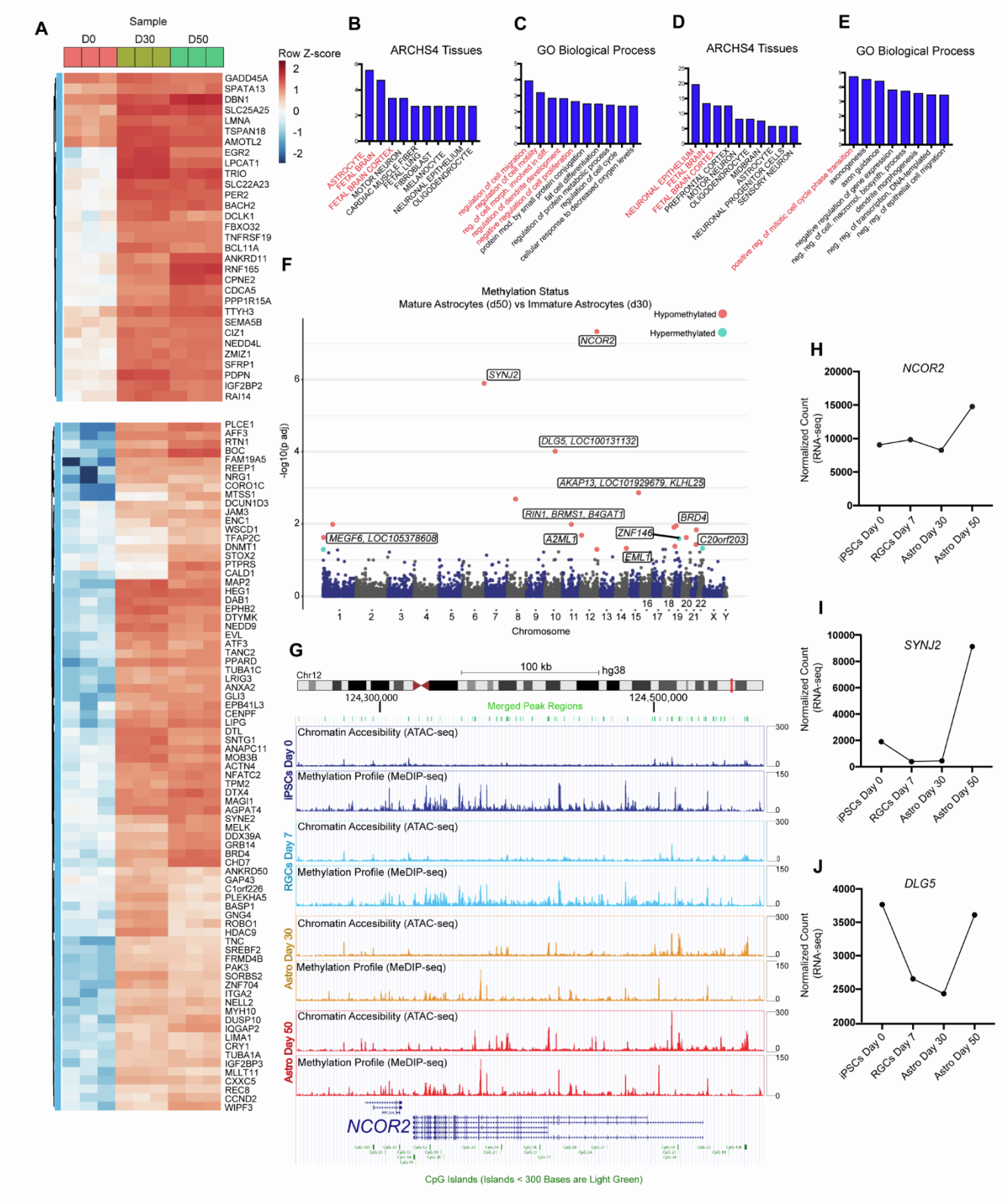
A
Sample
D0
D30
D50
Row Z-score
2
1
0
-1
-2
GADD45A
SPATA13
DBN1
SLC25A25
LMNA
TSPAN18
AMOTL2
EGR2
LPCAT1
TRIO
SLC22A23
PER2
BACH2
DCLK1
FBXO32
TNFRSF19
BCL11A
ANKRD11
RNF165
CPNE2
CDCA5
PPP1R15A
TTYH3
SEMA5B
CIZ1
NEDD4L
ZMIZ1
SFRP1
PDPN
IGF2BP2
RAI14
PLCE1
AFF3
RTN1
BOC
FAM19A5
REEP1
NRG1
CORO1C
MTSS1
DCUN1D3
JAM3
ENC1
WSCD1
TFAP2C
DNMT1
STOX2
PTPRS
CALD1
MAP2
HEG1
DAB1
EPHB2
DTYMK
NEDD9
EVL
ATF3
TANC2
PPARD
TUBA1C
LRIG3
ANXA2
GLI3
EPB41L3
CENPF
LIPG
DTL
SNTG1
ANAPC11
MOB3B
ACTN4
NFATC2
TPM2
DTX4
MAGI1
AGPAT4
SYNE2
MELK
DDX39A
GRB14
BRD4
CHD7
ANKRD50
GAP43
C1orf226
PLEKHA5
BASP1
GNG4
ROBO1
HDAC9
TNC
SREBF2
FRMD4B
PAK3
SORBS2
ZNF704
ITGA2
NELL2
MYH10
DUSP10
IQGAP2
LIMA1
CRY1
TUBA1A
IGF2BP3
MLLT11
CXXC5
REC8
CCND2
WIPF3
B
ARCHS4 Tissues
ASTROCYTE
FETAL BRAIN
FETAL BRAIN CORTEX
MOTOR NEURON
CARDIAC MUSCLE FIBER
FETAL LUNG
FIBROBLAST
MELANOCYTE
NEURONAL EPITHELIUM
OLIGODENDROCYTE
C
GO Biological Process
regulation of cell migration
regulation of cell motility
reg. of cell motility
regulation of cell morph. involved in diff.
regulation of dendrite development
negative regulation of cell proliferation
protein mod. by small protein conjugation
fat cell differentiation
regulation of protein metabolic process
regulation of cell cycle
cellular response to decreased oxygen levels
D
ARCHS4 Tissues
NEURONAL EPITHELIUM
FETAL BRAIN
FETAL BRAIN CORTEX
PREFRONTAL CORTEX
MOTOR NEURON
OLIGODENDROCYTE
MIDBRAIN
ASTROCYTE
NEURONAL PROGENITOR CELLS
SENSORY NEURON
E
GO Biological Process
positive reg. of mitotic cell cycle phase transition
axonogenesis
axon guidance
negative regulation of gene expression
neg. reg. of cell. macromol. biosynth. process
dendrite morphogenesis
neg. reg. of transcription, DNA-templated
neg. reg. of epithelial cell migration
F
Methylation Status
Mature Astrocytes (d50) vs Immature Astrocytes (d30)
Hypomethylated
Hypermethylated
NCOR2
SYNJ2
DLG5, LOC100131132
AKAP13, LOC101929679, KLHL25
RIN1, BRMS1, B4GAT1
BRD4
MEGF6, LOC105378608
A2ML1
ZNF146
C20orf203
EML1
-log10(p adj)
Chromosome
G
Chr12
100 kb
hg38
124,300,000
124,500,000
Merged Peak Regions
iPSCs Day 0
RGCs Day 7
Astro Day 30
Astro Day 50
Chromatin Accesibility (ATAC-seq)
Methylation Profile (MeDIP-seq)
NCOR2
CpG Islands (Islands < 300 Bases are Light Green)
H
NCOR2
Normalized Count (RNA-seq)
iPSCs Day 0
RGCs Day 7
Astro Day 30
Astro Day 50
I
SYNJ2
J
DLG5

Figure S4. Epigenetic changes during directed gliogenic differentiation

(A) Chromatin accessibility in hPSCs (day 0) and astrocytes (day 30, 50) considering the top 300 genes expressed by fetal and adult astrocytes (Zhang et al., 2016). Heatmaps show genes with strongest difference for chromatin accessibility. Dynamic chromatin changes identify two dominant gene clusters with open chromatin (upper panel showing 31 genes, lower panel showing 79 genes).

(B-E**)** Enrichr analysis of identified genes (*GO Biological process* and *ARCHS4 Tissues*).

(F) Manhattan plot displaying differential gene methylation with strongest difference between immature $GFAP^-$ (day 30) and mature astrocytes $GFAP^+$ (day 50). *NCOR2* hypomethylation in mature astrocytes (day 50) is the most significant hit when compared to immature astrocytes at day 30.

(G) UCSC Genome Browser plots showing chromatin accessibility and methylation profile of *NCOR2* gene loci across differentiation time-points. Note that *NCOR2* is hypermethylated in iPSC (Day 0) and RGCs (Day 7) and hypomethylation and open chromatin is detectable in astrocytes (day 30 and 50).

(H-J) Time-course transcriptomics (RNA-seq) showing strong expression of *NCOR2, SYNJ2* and *DLG5* by day 50. n = 3 independent astrocyte differentiation experiments (NCRM5).

Figure S5

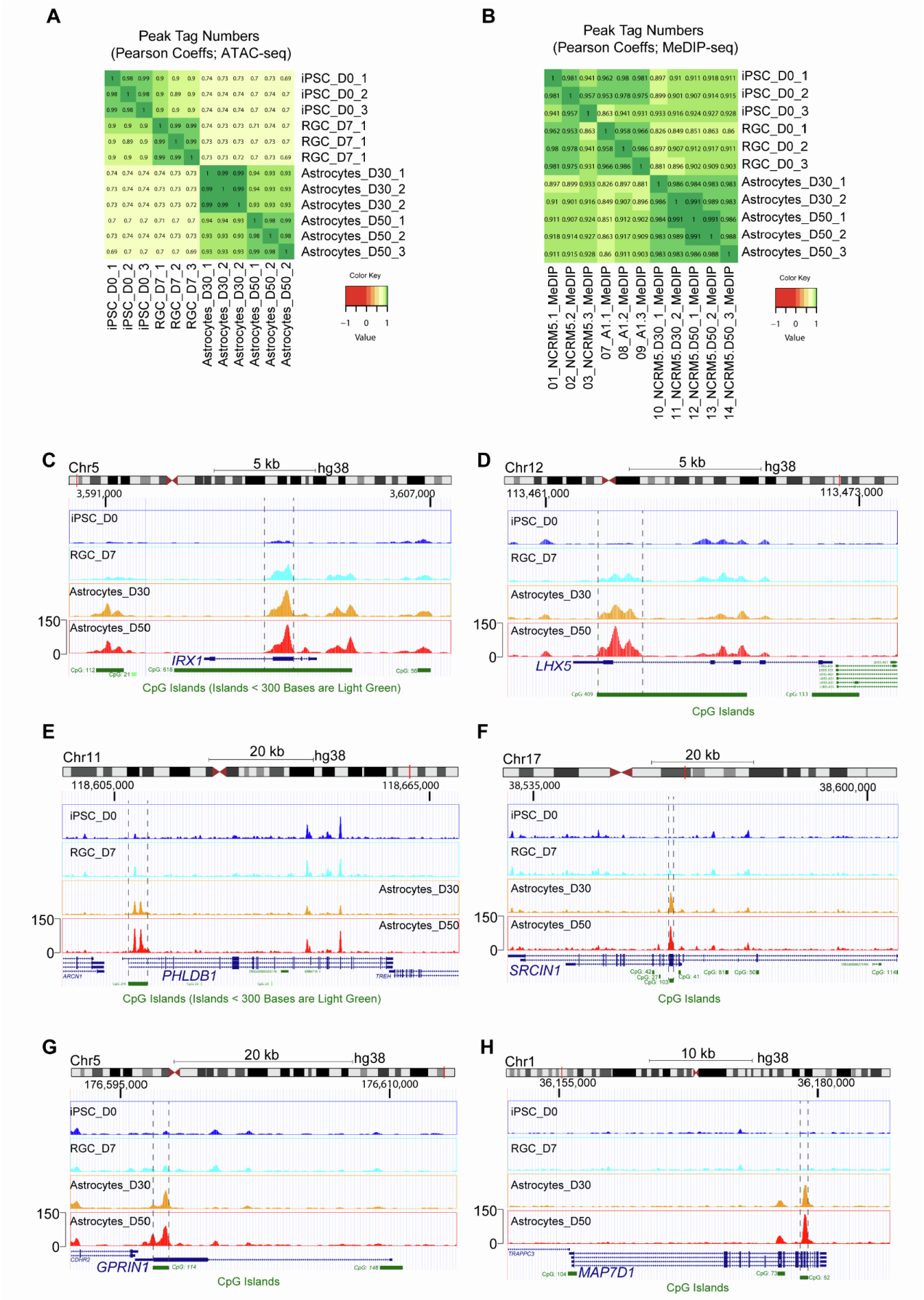
A
Peak Tag Numbers
(Pearson Coeffs; ATAC-seq)
iPSC_D0_1
iPSC_D0_2
iPSC_D0_3
RGC_D7_1
RGC_D7_1
RGC_D7_1
Astrocytes_D30_1
Astrocytes_D30_2
Astrocytes_D30_2
Astrocytes_D50_1
Astrocytes_D50_2
Astrocytes_D50_3
Color Key
Value
B
Peak Tag Numbers
(Pearson Coeffs; MeDIP-seq)
iPSC_D0_1
iPSC_D0_2
iPSC_D0_3
RGC_D0_1
RGC_D0_2
RGC_D0_3
Astrocytes_D30_1
Astrocytes_D30_2
Astrocytes_D50_1
Astrocytes_D50_2
Astrocytes_D50_3
01_NCRM5.1_MeDIP
02_NCRM5.2_MeDIP
03_NCRM5.3_MeDIP
07_A1.1_MeDIP
08_A1.2_MeDIP
09_A1.3_MeDIP
10_NCRM5.D30_1_MeDIP
11_NCRM5.D30_2_MeDIP
12_NCRM5.D50_1_MeDIP
13_NCRM5.D50_2_MeDIP
14_NCRM5.D50_3_MeDIP
Color Key
Value
C
Chr5
5 kb
hg38
3,591,000
3,607,000
iPSC_D0
RGC_D7
Astrocytes_D30
Astrocytes_D50
150
0
IRX1
CpG Islands (Islands < 300 Bases are Light Green)
D
Chr12
5 kb
hg38
113,461,000
113,473,000
iPSC_D0
RGC_D7
Astrocytes_D30
Astrocytes_D50
150
0
LHX5
CpG Islands
E
Chr11
20 kb
hg38
118,605,000
118,665,000
iPSC_D0
RGC_D7
Astrocytes_D30
Astrocytes_D50
150
0
PHLDB1
CpG Islands (Islands < 300 Bases are Light Green)
F
Chr17
20 kb
38,535,000
38,600,000
iPSC_D0
RGC_D7
Astrocytes_D30
Astrocytes_D50
150
0
SRCIN1
CpG Islands
G
Chr5
20 kb
hg38
176,595,000
176,610,000
iPSC_D0
RGC_D7
Astrocytes_D30
Astrocytes_D50
150
0
GPRIN1
CpG Islands
H
Chr1
10 kb
hg38
36,155,000
36,180,000
iPSC_D0
RGC_D7
Astrocytes_D30
Astrocytes_D50
150
0
MAP7D1
CpG Islands

Figure S5. Methylation signature of differentiated astrocytes.

(A,B) Correlation heatmaps showing Pearson coefficients of all pairwise comparisons, colored from dark green (high correlation) to yellow and red (low or no correlation). Lower correlation in chromatin accessibility across differentiation suggests more dynamic chromatin changes (A) relative to DNA methylation changes (B).

(C-H) UCSC Genome Browser plots showing gene loci hypermethylated in iPSC-astrocytes. Peaks marked by the dotted line are within the CpG island regions of (C) *IRX1*, (D) *LHX5*, (E) *PHLDB1*, (F) *SRCIN1*, (G) *GPRIN1* and (H) *MAP7D1*. n = 3 independent astrocyte differentiation experiments (NCRM5).

Figure S6

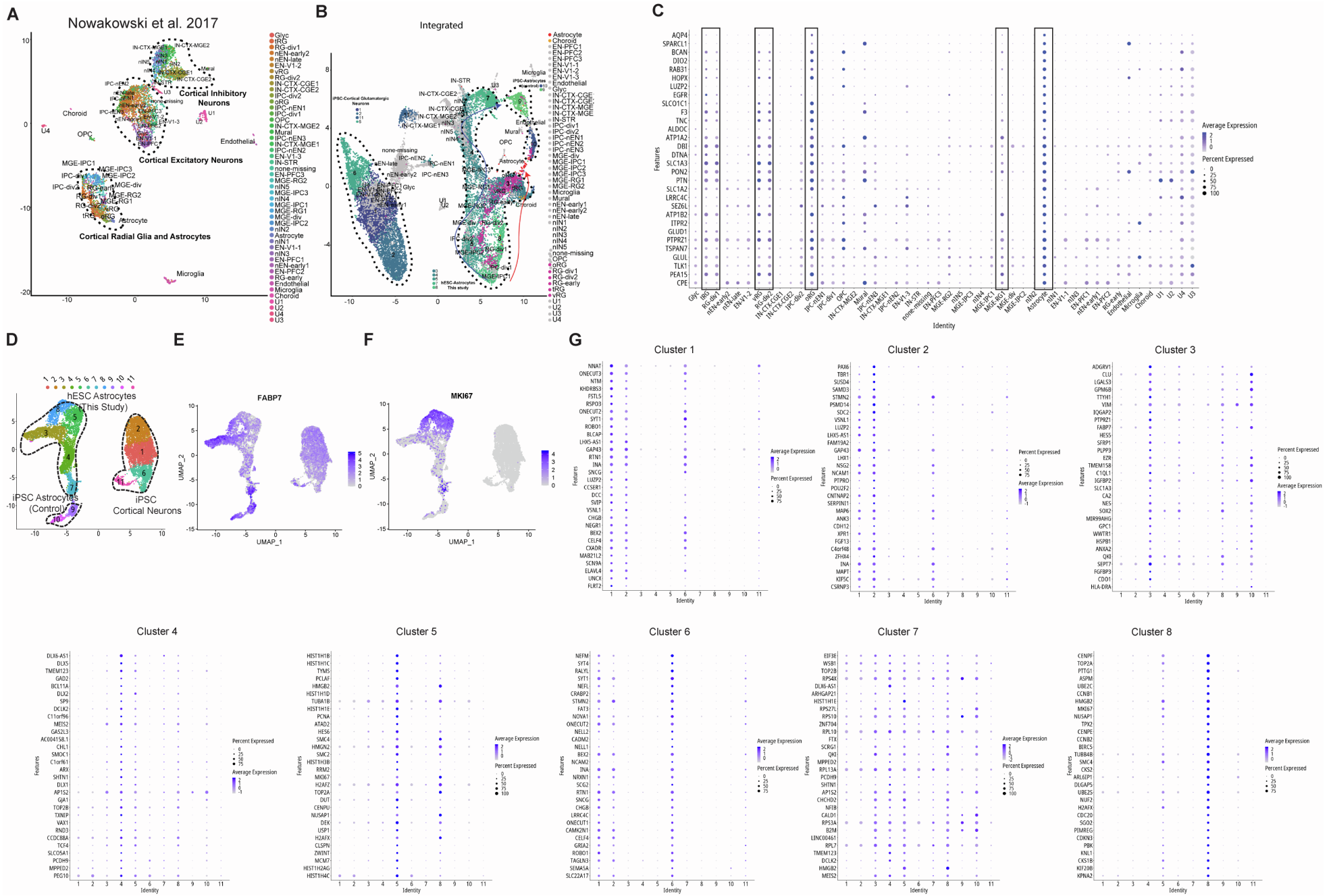
A
Nowakowski et al. 2017
Cortical Inhibitory Neurons
Cortical Excitatory Neurons
Cortical Radial Glia and Astrocytes
B
Integrated
C
Identity
Average Expression
Percent Expressed
D
hESC Astrocytes (This Study)
iPSC Astrocytes (Control)
iPSC Cortical Neurons
E
FABP7
F
MKI67
G
Cluster 1
Cluster 2
Cluster 3
Cluster 4
Cluster 5
Cluster 6
Cluster 7
Cluster 8

Figure S6. Integrated single-cell transcriptomic analysis of hPSC-astrocytes and comparison to human fetal cortex

(A) UMAP representation of 4,261 cells from the Nowakowski et al. study sampled across the human cortex development (gestational week 5 – 37) outlines three broad clusters excitatory neurons, inhibitory neurons, and radial glia/astrocyte.

(B) UMAP showing the integration of hPSC-derived astrocytes and cortical excitatory neurons with a published dataset (Nowakowski et al., 2017). Due to the differences in the number of profiled cells hPSC-cluster sizes were significantly larger. Note that hPSC-derived astrocytes cluster together with radial glia and astrocytes.

(C) Feature plot depicting the top 30 genes expressed in human fetal astrocyte cluster and high similarity to radial glia clusters (boxed) (adopted from Nowakowski et al., 2017).

(D) UMAP representation of unbiased clustering of hPSC-astrocyte samples. Seurat analysis identified 8 different clusters.

(E-F) Feature plots demonstrating *FABP7* and *MKI67* expression across astrocyte clusters.

(D) Dot plots showing the top 30 gene features for each of the astrocyte clusters.

Data from 4261 single cells (Nowakowski et al., 2017) was used for data integration. Data from 6138 single cells from derived astrocytes (WA09) and 744 control astrocytes (FUJIFILM CDI). Single-cell RNA-seq data were analyzed in the Seurat R package.

Figure S7

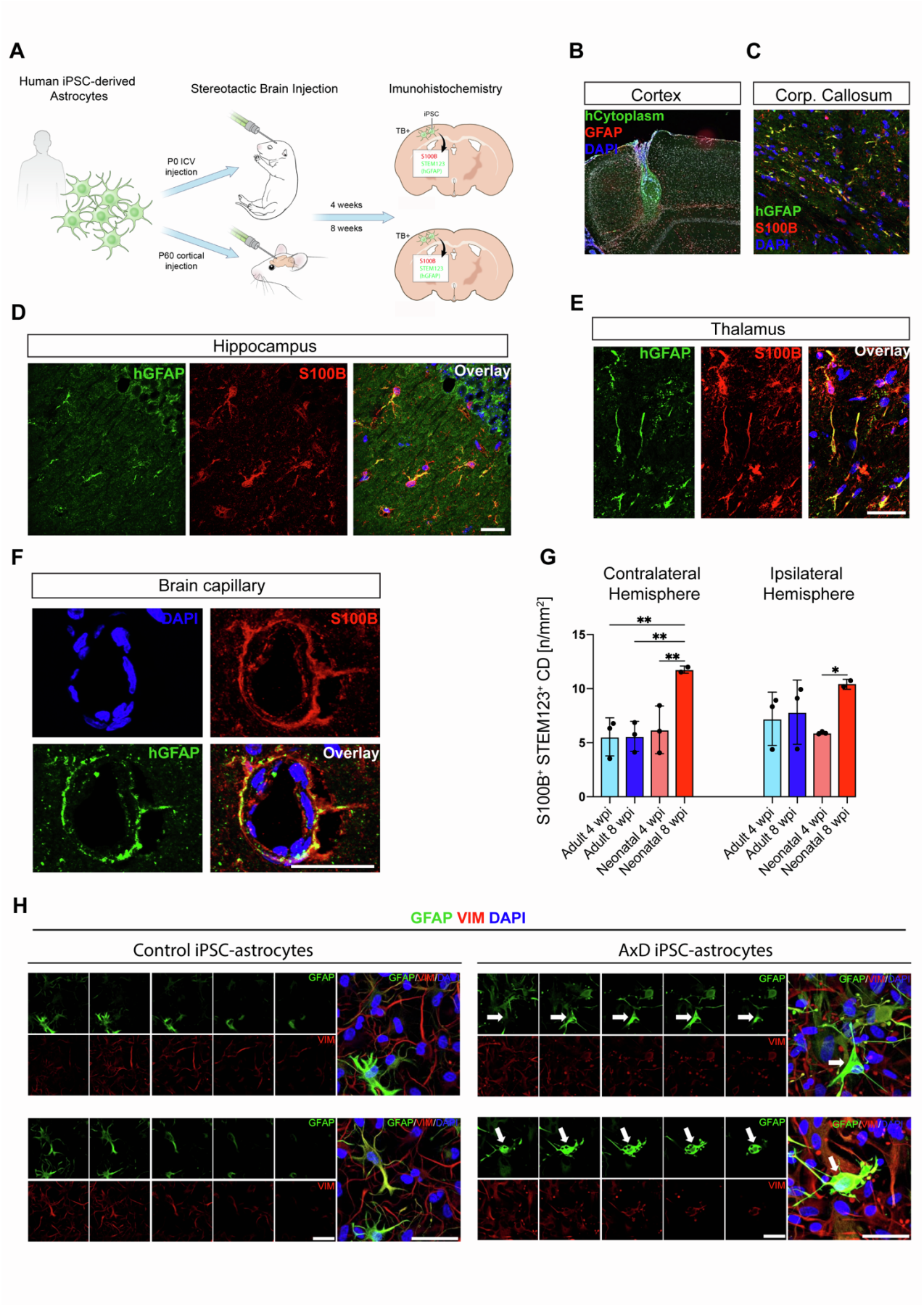
A
Human iPSC-derived Astrocytes
Stereotactic Brain Injection
Imunohistochemistry
P0 ICV injection
P60 cortical injection
4 weeks
8 weeks
iPSC
TB+
S100B
STEM123
(hGFAP)
B
Cortex
hCytoplasm
GFAP
DAPI
C
Corp. Callosum
hGFAP
S100B
DAPI
D
Hippocampus
hGFAP
S100B
Overlay
E
Thalamus
hGFAP
S100B
Overlay
F
Brain capillary
DAPI
S100B
hGFAP
Overlay
G
Contralateral Hemisphere
Ipsilateral Hemisphere
S100B+ STEM123+ CD [n/mm2]
15
10
5
0
**
**
**
*
Adult 4 wpi
Adult 8 wpi
Neonatal 4 wpi
Neonatal 8 wpi
H
GFAP VIM DAPI
Control iPSC-astrocytes
AxD iPSC-astrocytes
GFAP
VIM
GFAP/VIM/DAPI

Figure S7. Brain engraftment of human astrocytes and analysis of iPSC-derived astrocytes from AxD patient

(A) Schematic of experimental design and treatment groups.

(B) Human iPSC-astrocytes (NCRM5) transplanted into the adult mouse cortex (4 weeks post-grafting) show strong immunoreactivity against human cytoplasmic marker STEM121 and GFAP.

(C) Immunostaining for human-specific GFAP (STEM123 antibody) and S100B detect migratory cells in the corpus callosum.

(D-E) Immunostaining for human specific GFAP (STEM123) showing cells in the thalamus and hippocampus indicating long-distance migration of astrocytes grafted into the cortex.

(F) Human GFAP-expressing astrocytes surrounding a blood vessel in the mouse brain parenchyma.

(G) Quantification of $S100B^+$ and $hGFAP^+$ co-labeled cells in the ipsi- and contralateral hemispheres of adult and neonatal mice at 4- and 8-weeks post-grafting (n = 3 animals per group).

(H) Confocal images (1 μm optical sections) showing $GFAP^+$ aggregates and aberrant astrocyte morphology in AxD astrocytes (GM16825) but not control astrocytes (NCRM5).

Scale bars (B-F) 100 μm, (H) 50 μm.

Movie S1. Slow spontaneous calcium transients in astrocytes

Video-microscopy of iPSC-derived astrocytes (day 50, LiPSC GR1.1) loaded with calcium dye (FLIPR Calcium 6 kit). Note the spreading of calcium transients across the cell culture.

Movie S2. Slow spontaneous calcium transients in control astrocytes

Video-microscopy of iCell astrocytes (FUJIFILM CDI) loaded with calcium dye (FLIPR Calcium 6 kit). Note that these control astrocytes behave similarly to the iPSC-derived astrocytes shown in Movie S1.

Supplementary Table 1

Protein densitometry values associated with Figures S2 and S3.

Experimental Procedures

Differentiation of hPSCs into RGCs and astrocytes

For RGC differentiation, hPSCs were detached using 0.5 mM EDTA and plated at 10.000 cell/cm^2 density on a VN-coated surface in E8 medium supplemented with CEPT (day -1). The following day medium was replaced with freshly prepared Astro-1. On day 3, cells were dissociated using 0.5 mM EDTA and 20.000 cell/cm^2 were plated on a VN-coated surface in Astro-1 medium supplemented with CEPT for 24 h. Daily Astro-1 medium changes were performed to generate neural rosettes by day 7. For patterning RGCs into OTX2$^+$ neural progenitors, 0.8 μM CHR99021 (Tocris, 4423) + 100 ng/mL FGF8b (R&D Systems, 423-F8) were added to Astro-1 medium between days 7-15. For patterning RGCs into HOXA2$^+$ progenitors, 1 μM CHR99021 (Tocris, 4423) was added to Astro-1 medium between days 7-15.

For astrocyte differentiation, RGCs were maintained in Astro-1 medium until day 15, with daily medium changes. Cell passaging was performed on days 7, 11, and 14 using Accutase and at each passaging step 30,000 cells/cm^2 were plated on VN-coated plates in Astro-1 medium supplemented with CEPT for 24 h. On day 15, medium was replaced by Astro-2. Medium changes were performed daily with passaging on day 18 and 23, and 40.000 cells/cm^2 were plated on VN-coated plates and maintained until day 30. On day 30, cells were either cryopreserved in Astro-2 medium supplemented with 10% DMSO and CEPT or further matured in Astro-3 medium until day 50.

For astrocyte maturation, day-30 astrocytes were plated on Geltrex (Thermo Fisher Scientific, A1569601) at 50.000 cells/cm^2 and maintained in Astro-3 medium until day 50. Astro-3 medium was based on DMEM/F12 medium supplemented with N2, B27 with vitamin A, 1% lipid supplement (Gibco) and JAGGED-1, DLL-1, LIF, CNTF all at 10 ng/ml concentration, hNRG1/EGF domain 20 ng/ml, 2 μM forskolin, 200 nM phorbol-ester, 40 ng/ml triiodothyronine and 200 μM ascorbic acid. Cultures were passaged (1:2 ratio) on day 37 and 43, respectively. On day 50, cells were cryopreserved in Astro-3 medium supplemented with 10% DMSO and CEPT.

For robotic astrocyte differentiation, 1.75 million hPSCs were plated in T175 flasks and cultured in the CompacT SelecT system (Sartorius) and Astro-1, Astro-2, and Astro-3 media were applied as described above. All media

changes (Days 0-50) were performed by the robotic instrument throughout the cell differentiation process. Cell culture flasks were only briefly removed from the system for offline centrifugation to remove Accutase that was used for cell dissociation.

Differentiation with Astro-1/Astro-2 versus alternative media

To generate NFIA$^+$ RGCs, cells were treated for 7 days in Astro-1 and 7 days in Astro-2, or the same basal medium (DMEM/F12; N2; B27 without vit. A) supplemented with 25 ng/ml EGF (R&D systems, 236-EG), 25 ng/ml FGF2 (R&D systems, 3718-FB) and 2% FBS (Gibco, A4766801) and 10 ng/ml LIF. Cells were passaged on days 11, 14 and 18 and plated at 30.000, 40.000 and 40.000 cells/cm^2. At day 21, cells were washed in PBS, harvested using a cell scraper and cell pellets frozen on dry ice after centrifugation and removal of PBS (Figure 2A and 2B).

To compare NFIA induction across 6 treatment combinations (Figure S3), three independent hPSC lines (WA09 hESC, NCRM5 and LiPSC GR1.1) were treated as follows:

i. BMP inhibitor LDN193189 (100nM) from day 0-14 followed by Astro-2 (day 14-21);

ii. LDN193189 (100nM) and TGFß inhibitor A83-01 (2 μM) for the first 7 days, followed by EGF/FGF2 (25 ng/ml each), day 7- 21.

iii. Astro-1/Astro-2 combination following the described protocol.

iv. Astro-1 supplemented with EGF/FGF2 (25 ng/ml each)/Astro-2 supplemented with EGF/FGF2 (25 ng/ml each); v. Astro-1/Astro2 supplemented with EGFR inhibitor Afatinib (1 μM) and FGFR 1/2/3 inhibitor PD173074 (25 nM).

vi. Astro-1 with removal of NOTCH ligands (DLL-1 and Jagged-1)/ Astro-2 with removal of NOTCH ligands (DLL-1 and Jagged-1).

Importantly, the same basal media components and passaging timepoints, and other experimental steps were performed across all conditions. At day 21, cells were washed in PBS, and harvested using a cell scraper and cell pellets frozen on dry ice after centrifugation and removal of PBS.

Immunocytochemistry

Cells cultured in 6-, 24- or 96-well plates or 8 chamber slides (Ibidi) were fixed with 4% PFA diluted in PBS for 15 min and washed 3 times with PBS (5 min each). Blocking was performed with 4% donkey serum and 0.1% Triton-X in PBS for 1h at room temperature on a shaker. All primary antibodies in this study were applied overnight at 4°C. Next day, cultures were washed 3 times with PBS and appropriate secondary antibodies were applied for 1h at room temperature. Fluorescence images were taken with the Leica DMi8 epifluorescence and Zeiss LSM 710 confocal microscopes using appropriate filters. Primary antibodies used for immunocytochemistry are as follows: mouse anti-PAX6 1:200 (BD Biosciences, 561462,), rabbit anti-FABP7 (BLBP) 1:200 (EMD Millipore, ABN14), rabbit anti-CD44 1:400 (Abcam, ab157107), rat anti-CD44 1:100 (Abcam, A25528), mouse anti-VIMENTIN 1:500 (DAKO, M0725), rabbit anti-NFIA 1:250 (Novus, NBP-1-81406), rabbit anti-S100-beta 1:100 (Abcam, ab52642), mouse anti-TUJ1 1:1000 (BioLegend, 801201), rabbit anti-GFAP 1:1000 (DAKO, Z0334), rabbit anti-SYNAPSIN-1 1:500 (Synaptic Systems, 106-011), rabbit anti-ASPM 1:100 (Novus, NB-100-2278), rabbit anti-FAT1 1:100 (Millipore-Sigma, HPA023882) and mouse anti-Pan-Neuronal Marker (PNM) 1:200 (EMD Millipore, MAB2300), goat anti-OTX2 1:50 (R&D systems, AF1979), rabbit anti-HOXA2 1:200 (Sigma Aldrich, HPA078220), OLIG2 (Millipore Sigma, AB9610) . The following secondary antibodies were used: donkey anti-mouse Alexa 568 (1:500, A-10037, Thermo Fisher Scientific) and donkey anti-rabbit Alexa Fluor 488 (1:500; A-21206, Thermo Fisher Scientific).

Western blot

The Wes and Jes automated Western blotting systems (Protein Simple) were used for quantitative analysis of protein expression as described previously(Chen et al., 2021; Tristan et al., 2020; Tristan et al., 2021). Western blots are displayed by lanes in virtual blot-like images. Briefly, cells were harvested by scraping, pelleted, washed with PBS, flash frozen using dry ice and stored at -20 °C until processed. Cell pellets were resuspended in RIPA buffer (Thermo Fisher Scientific) supplemented with halt protease inhibitor cocktail (Thermo Fisher Scientific) and lysed by sonication. Lysates were cleared of debris by centrifugation at 14,000 g for 15 min and quantified using the BCA protein assay kit (Thermo Fisher Scientific). Lysates were diluted 1:4 with 1X sample buffer (Protein Simple). Protein quantification was performed using the 12-230 kDa 13 25-lane plate (PS-MK15; Protein

Simple) in a Wes Capillary Western Blot analyzer according to the manufacturer's recommendation. Protein quantification was done using the Compass software. Primary antibodies used are as follows: mouse anti-GAPDH 1:2,000 (Santa Cruz, sc25778,), rabbit anti-PAX6 1:20 (BioLegend, 901301), rabbit anti-FAT1 1:20 (MilliporeSigma, HPA023882), rabbit anti-ATF4 1:50 (Cell Signaling Technology, D4B8), rabbit anti LC3 A/B 1:50 (Cell Signaling Technology, D3U4C), rabbit anti-ATG3 1:50 (Cell Signaling Technology, 3415), rabbit anti-ATG5 1:50 (Cell Signaling Technology, D5F5U), rabbit anti-TDP43 total 1:50 (Cell Signaling Technology, 89789) and rabbit anti-phospho-TDP43 1:50 (Thermo Fisher Scientific, 22309-1-AP), mouse anti-TUBB3 (TUJ1) 1:50 (BioLegend, MMS-435P), rabbit anti-CD133 1:50 (Abcam, ab19898), rabbit anti-S100-beta 1:50 (Abcam, ab52642), mouse anti-Synaptophysin-1 1:50 (Synaptic Systems, 101 011), rabbit anti phospho-AKT (Cell Signaling Technology, 4060S), rabbit anti phospho-p44/42 MAPK (Cell Signaling Technology, 4376S), rabbit anti AKT (Cell Signaling Technology, 9272), rabbit anti p44/42 MAPK (Cell Signaling Technology, 4695), rabbit anti EGFR (Cell Signaling Technology, 4267).

Transmission Electron Microscopy (TEM)

Astrocytes differentiated from hPSC (day 30 and 50) and cultured in 6-well plates (1 million cells per well) and control astrocytes (FUJIFILM CDI, 01434) were fixed by replacing the media with 2.5% glutaraldehyde in PBS (pH 7.2–7.4) for 60 minutes at room temperature. Sample processing for electron microscopy and imaging (Hitachi, H7659) was performed by the Electron Microscopy Laboratory of Leidos Biomedical Research, NCI, Frederick, MD.

RNA Scope Fluorescent Multiplex Assay

One day before fixation (day 6), Astro-1 or dSMADi treatment cells were seeded on 4-chamber slides (Ibidi) coated with VN in Astro-1 medium or dSMADi at a high-density that allowed cells to be 80–90% confluent at the time of fixation. After removal of growth medium, cells were briefly washed with PBS and fixed in 10% PFA for 30 mins. Following fixation, cells were rinsed twice in PBS before dehydration by submerging in a series of ethanol solutions (50%, 70% and 100%). Rehydrated cells were pretreated to block endogenous peroxidase activity and optimally permeabilize samples to allow probe access to target RNA using pretreatment kit (ACD,

322380). The hybridization was performed according to RNAscope® Fluorescent Multiplex Kit protocol (ACD, 320293) using custom made RNAscope® Probe- Hs-BIRC5 (ACD, 465361) and positive control RNAscope® Positive Control Probe- Hs-POLR2A (ACD,310451). Fluorescence images were taken with the Leica DMi8 epifluorescence microscope.

Co-culturing astrocytes and neurons

For co-culture experiments, iPSC-derived glutamatergic or motor neurons (FUJIFILM CDI, R1061, R1051) were plated on Geltrex-coated plates (100,000 cells per cm^2) and placed into the incubator (37 °C) for 45 mins to allow cell attachment. Then, 33,000 astrocytes were added per cm^2 to achieve a 1:3 ratio. The neuronal medium recommended by the vendor (FUJIFILM CDI) was supplemented with 10 ng/ml LIF (R&D Systems), 10 ng/ml CNTF (R&D Systems) and 1% lipid supplement (Gibco). CEPT was included for the first 24 h. Co-cultures were maintained for up to 21 days prior to fixation with 4% PFA and immunostaining. Control astrocytes (FUJIFILM CDI, 01434) are >95% pure cultures with the expression of typical markers (e.g., S100β and GFAP).

Brain spheroids and oligodendrocyte precursor differentiation from RGCs

Cortical spheroids were cultured based on a published method (Marton et al., 2019) with the exception that spheroid formation was initiated using RGCs. Briefly, RGCs (WA09) were dissociated at day 7 using Accutase (Thermo Fisher Scientific) and plated in 96-well ultra-low attachment (ULA) round-bottom plates (Corning) at a density of 20,000 cells per well in expansion media consisted of DMEM/F12-Glutamax(Gibco) media with 1% N2 supplement (Gibco), 2% B27 without vitamin A (Gibco), 20 ng/mL human EGF (R&D) and 20 ng/mL human FGF (R&D). The cells were treated with the CEPT cocktail (Chen et al., 2021) for the first 24 h, followed by media change with expansion media. At day 3, the aggregated cells were transferred to ULA 24-well plates (Corning) at density of 1 sphere/well with 500 μl of expansion media. The medium was changed every other day. At day 7, the medium was changed to maturation medium which was consisted of DMEM/F12-Glutamax (Gibco) with 1% N2 supplement (Gibco), 2% B27 (Gibco), 25 ng/mL human BDGF (R&D), 25 ng/mL human GDNF (R&D), 25 ng/mL human NT-3 (R&D), 200 μM ascorbic acid (Tocris), and 1mM dbCAMP (Tocris). All cultures were maintained at 37 °C under humidified 5% CO_2 and atmospheric oxygen. Organoids were fixed in 4% PFA at

room temperature for 20 min, washed with PBS three times, and incubated in 30% sucrose at 4°C overnight. Tissues were embedded in O.C.T. compound (Fisher Scientific), cut into 10-μm sections, and mounted on microscope slides. For immunohistochemical analysis, sections were permeabilized and blocked with 0.3% Triton X-100 and 5% BSA in PBS for 1h. Slides were mounted with ProLong Glass Antifade Mountant with NucBlue Stain (Thermo Fisher Scientific). Fluorescence images were taken with the Zeiss LSM 710 confocal microscope using appropriate filters.

For oligodendrocyte precursor cell differentiation in monolayer cultures, hPSC-derived RGCs (WA09; LiPSC GR 1.1) were differentiated for 21 days, with passaging every 4-5 days (30.000 cell/cm^2), using SAG21k (0.5 μM), EGF/FGF2 (25 ng/ml each) and RA (1 μM) added to Astro-1 medium. After 3 weeks (passage 5) immunocytochemistry was performed for OLIG2 expression.

Multi-electrode array

Electrophysiology was performed using the Maestro platform (Axion Biosystems). Glutamatergic neurons (FUJIFILM CDI, R1062) were plated at a density of ~5 million neurons per cm^2 in complete neuronal media as recommended by the vendor: BrainPhys Neuronal Medium (STEMCELL Technologies, 05790) supplemented with iCell Neural Supplement B (FUJIFILM CDI, M1029) and iCell Nervous System Supplement (FUJIFILM CDI, M1031), N2 (Gibco), 10 µg/mL laminin (Thermo Fisher Scientific), 10 ng/ml LIF (R&D Systems), 10 ng/ml CNTF (R&D Systems) and 1% lipid supplement (Gibco) and CEPT. 48-well plates with electrodes were coated with 0.1% polyethylenimine (PEI). Motor neurons (FUJIFILM CDI) were plated at a density of ~5 million neurons per cm^2 in complete medium containing CEPT. For co-culture experiments with neurons, iPSC-astrocytes generated at NCATS were compared to control iCell Astrocytes (FUJIFILM CDI, R1092). Plating of astrocytes and neurons in 1:3 ratio is described above. 48-well MEA plates were coated with Geltrex (Gibco). Twenty-four hours post-plating, fresh medium was added and CEPT was removed and then 50% media changes were performed every 2-3 days. Electrophysiological recordings were performed daily for 10 min.

High-throughput calcium imaging

hPSC-derived astrocytes were plated onto Geltrex-coated 96-well plates with transparent bottom (Greiner) and maintained in Astro-3 media for 5-7 days with daily media changes prior to calcium imaging. Calcium imaging was performed on the FLIPR Penta high-content calcium imager (Molecular Devices). On the day of the experiment, cultures were prepared according to the instructions detailed in the FLIPR Calcium Assay 6 kit (Molecular Devices). Briefly, cells were loaded using 100 µl of prepared loading buffer without removing media portion (100 µl) and incubated for 2 h at 37 °C. After incubation, the 96 well cell plate was transferred to the FLIPR instrument and the experiment was initiated by taking 200 measurements of basal signal levels followed by administration of DMSO, L-glutamate (100 µM), ATP (30 µM) or KCl (65 mM), and recording of 600 measurements (read interval 1/s). For IP3R profiling experiments, 1h pretreatment with different dosages of 2-APB (Tocris, 1244) was performed during the second hour of incubation with the loading buffer.

Glutamate uptake assay

hPSC-derived astrocytes, control astrocytes (FUJIFILM CDI), mouse astrocytes (ScienCell) and hPSCs (negative control) were plated onto Geltrex-coated 96-well plates (Corning) and maintained in Astro-3 medium (astrocytes) or E8 medium (hPSCs) for 5-7 days with daily media changes prior to performing glutamate uptake assay. On the day of the experiment, cells were first incubated for 30 min in Hank's balanced salt solution (HBSS) buffer without calcium and magnesium (Gibco), prior to 3 h incubation with 100 µM L-glutamate in HBSS with calcium and magnesium (Gibco) to allow glutamate uptake by cells. After 3 h, medium/supernatant was analyzed with a colorimetric glutamate assay kit (Sigma-Aldrich, MAK004) according to the manufacturer's instructions.

Cytokine stimulation of astrocytes

hPSC-derived astrocytes, control astrocytes (FUJIFILM CDI), mouse astrocytes (ScienCell) and hPSCs were plated onto Geltrex coated 96 well plates (Corning) and maintained in Astro-3 medium (astrocytes) or E8 medium (hPSCs) for 5 – 7 days with daily medium changes prior to performing cytokine stimulation. On the day of the experiment, cells were treated with 3 ng/ml IL-1α (MilliporeSigma, SRP3310), 30 ng/ml tumor necrosis factor (Cell Signaling Technology, 8902SF) and 400 ng/ml C1q (MyBioSource, MBS143105) for 24 h. The

following day, medium was isolated, spun down to remove debris, and human complement C3 levels were measured using the Human Complement C3 ELISA Kit (Abcam, ab108823) following the manufacturer's instructions.

Live-cell metabolic assays using the Seahorse XF analyzer

The oxygen consumption rate (OCR) and extracellular acidification rate (ECAR) were analyzed using a Seahorse XF-96 analyzer (Agilent) according to the manufacturer's protocol. iPSC-astrocytes from Alexander disease (GM16825) and control astrocytes (NCRM5) were maintained in Astro-3 medium or Astro-3 medium supplemented with 3 ng/ml IL-1α (MilliporeSigma, SRP3310), 30 ng/ml tumor necrosis factor (Cell Signaling Technology, 8902SF) and 400 ng/ml C1q (MyBioSource, MBS143105) for 24 h prior to experiment. OCR and ECAR values were normalized to total cells per well.

High-content imaging and image analysis

hPSC (WA09, LiPSC GR 1.1, NCRM5) were seeded at 20.000 cells/cm2 in E8 with CEPT (day -1) and differentiated in the presence of Astro-1 or dSMADi (100 nM LDN-193189 + 2 μM SB431542) for 7 days in 6 well plates. For each cell line, 3 replicate wells were included in the experiment. On day 3, cells were dissociated (0.5 mM EDTA) and 20.000 cell/cm^2 was plated on VN-coated surface in Astro-1 medium supplemented with CEPT. Daily medium changes were performed using Astro-1 or dSMADi medium and cells were fixed in 4% PFA on day 7. After immunocytochemistry was performed against ZO-1 and FABP7, the central area of each well was imaged using Opera Phenix (PerkinElmer) high-content confocal imager (10x magnification). Images were imported from Opera Phenix to Columbus image analysis system (Perkin Elmer) and batch analysis was performed after ROI mask parameters were defined. Rosette lumen morphology was subjectively observed/identified as a connected image region, which was the size of multiple cells, where there was minimal DAPI staining and high relative levels of ZO-1 staining. The steps of the customized automated algorithm, which operates within the PerkinElmer Columbus high-content analysis platform, performed the following functions: 1) image filtering to enhance the local cluster pattern of ZO-1 staining, 2) blob detection [commercial proprietary algorithm, PerkinElmer] based on the enhanced ZO-1 image, 3) measurement of DAPI intensity and ZO-1

staining intensity within each blob region, 4) selection of blob regions as 'rosette lumen ROI masks' by thresholding DAPI intensity value and ZO-1 staining intensity value. DAPI and ZO-1 intensity thresholds were set empirically during assay development, and the same threshold values were applied to generate all batch analysis results.

Glycogen staining (Periodic Acid-Schiff)

hPSC-derived astrocytes and control astrocytes (FUJIFILM CDI) were washed with ice-cold PBS and fixed with ice-cold methanol for 5 min. After fixation, the Periodic Acid-Schiff staining kit (MilliporeSigma, 101646) was used according to manufacturer. Autofluorescence emitted by PAS-labeled granules was captured by using the Leica DMi8 epifluorescence microscope at 568 nm wavelength.

Cell transplantation

Adult male and female C57Bl/6J mice were purchased from The Jackson Laboratory (Maine, USA) at 8 weeks of age and grouped housed in same gender in OptiMice ventilated racks. Mice were acclimated to the vivarium for a week prior to injections. For neonatal injections, pregnant C57Bl6/J mice (E13 – E15) were purchased from The Jackson Laboratory. Mice were housed in OptiMice ventilated racks. Pups were weaned at 21 days and grouped housed by gender and treatment group. Over the course of the study, 12/12 light/dark cycles were maintained. The room temperature was maintained at 20-23 ºC with a relative humidity of around 50%. Chow and water were provided ad libitum.

On the day of cell grafting, media was aspirated from the T25 flasks with iPSC-derived astrocytes (day 30) and 2 ml of Accutase (room temperature) was added per flask and incubated for 7 min, after which the cells were monitored by microscopy every 2-3 minutes until rounding of the cells was observed. Astrocytes were then pooled in sterile conical tubes and centrifuged at 300 g at room temperature for 3 min. Cell pellets were gently resuspended in 1-5 ml DPBS. Cell numbers were counted with Countess Counter (Thermo Fisher Scientific) with Trypan Blue staining. Live cell numbers were calculated, and the cell suspension was supplemented with CEPT. After resuspension, cells were kept on ice. 3 μl of suspension (50.000 cells) per hemisphere was injected.

To perform intracerebroventricular (ICV) injections into newborn mice (postnatal day 1), animals were exposed to cryoanesthesia and injected with a dose volume of 1µl/g solution. A micro-liter calibrated sterilized glass micropipette was used that was attached to a 10 µl Hamilton syringe. The needle tip was adjusted to correct length for a 2 mm penetration into the skull. The immobilized mouse was firmly grasped by the skin behind the head. A fiber optic light was used to illuminate relevant anatomical structures for guidance. The needle was penetrated, perpendicularly, 2 mm into the skull, for ICV at a location approximately 0.25 mm lateral to the sagittal suture and 0.50-0.75 mm rostral to the neonatal coronary suture. Dosing solution was dispensed slowly (about 1µl/sec). Once the dose was administered, the needle was slowly removed (about 0.5 mm/sec) to prevent back flow.

For grafting into adult mice, animals were placed in an induction chamber to receive anesthesia using 2% isoflurane in the air mixture. The fur of the scalp and anterior back was clipped, and the animal was placed back into the induction chamber. The animal was then placed in a stereotactic apparatus such that the 180 ear bars were in the ear canals and the incisors were in the tooth bar of the mouse adapter. Surgical planes of anesthesia were maintained with 2% isoflurane by a nose cone fitted to the stereotaxic instrument. The scalp was prepared for surgery by cleaning the clipped injection site with Povidone iodine and rinsed with 70% ethanol. Mice were checked for a withdrawal reflex by pinching the hind foot to assess for anesthetic depth before an incision was made. A 1-1.5 cm slightly off-center incision was made in the scalp. The subcutaneous tissue and periosteum were scraped from the skull with sterile cotton tipped applicators. The guide cannula attached to stereotaxic arm was positioned over Bregma and this coordinate is considered the zero point. The guide cannula was moved to the appropriate anterior/posterior (-1.9) and medial/lateral (+/- 0.3) coordinates. Mice were infused with cells bilaterally in the cortex at a depth of (-2.5) with 3 ul on each side, at a rate of 0.3 µl/min with a 4 min rest period following injection. Overall, one adult mouse and 3 pups died post-injection.

For brain collection, animals were randomly split into two groups for collections at 2 time points after engraftment: 1) 4 weeks post grafting; 2) 8 weeks post grafting. Mice were deeply anesthetized with pentobarbital and monitored for loss of reflexes until all the responses to external stimuli cease (verified by a toe pinch). The abdominal cavity was opened, followed by opening of the chest cavity. A blunt-end perfusion needle was inserted into the left ventricle and forwarded toward the ascending aorta. Immediately after, a small incision was made

on the right atria. The perfusion needle was connected to an automated perfusion pump through a catheter system for a continuous administration of ambient temperature phosphate-buffered saline (PBS; 20 mM, pH 7.4 at room temperature). Approximately 40 ml of PBS was perfused at a rate of 10 ml/min. Saline flush was followed by perfusion with freshly prepared phosphate buffered 4% PFA. Brains were harvested and post-fixed overnight in freshly prepared phosphate buffered 4% PFA then transferred to 15% sucrose/PBS solution.

For immunohistochemistry, cryosectioned brains were stained to detect expression of human cytoplasmic marker STEM121 (TaKaRa, Y40410) and human-specific GFAP marker STEM123 (TaKaRa, Y40420). As general astrocyte markers GFAP (DAKO, z0334) and S100B (Abcam, ab52642) were used.

For quantitative image analysis, four different ROIs were manually drawn in Image J and either concentrated on the cerebral cortex around the graft injection site or delineated the entire hemisphere. A bilevel black and white DAPI mask was stored for every ROI and image. The inverted DAPI mask was mathematically subtracted from the S100B original image channel. A mask of $S100B^+$ nuclei was stored for each image and ROI. The mask of $S100B^+$ nuclei was mathematically added to the original S100B image. This procedure allowed for extraction of the entire shape of cells around the $DAPI^+$ and $S100B^+$ nucleus as far as labeled. This approach guaranteed that only structures that can be measured are those directly attached, hence, segmented processes were not included. A mask reflecting this core shape of $S100B^+$ astrocytes was saved for each image and ROI. The inverted S100B cell mask was subtracted from the original STEM123 image and signal above threshold and size restrictions overlapping with $S100B^+$ morphology was counted using restrictions and “fill holes” and “pixel connect” option to assure that for every IR area one object is counted (not to bias objects density). All cell transplantation experiments were performed by PsychoGenics (Paramus, NJ, USA) as part of a service agreement. The protocol was approved by the Committee on the Ethics of Animal Experiments of PsychoGenics and NIH.

Bulk RNA-seq

hPSCs and differentiating cells at different time points were lysed using buffer RLT+ (1053393, Qiagen) supplemented with 2-mercaptoethanol (63689, Millipore-Sigma) directly in wells and RNA was extracted and purified using RNeasy Plus Mini Kit (74136, Qiagen) according to the manufacturer’s instruction. QIAcube

automated workstation was used for the extraction (Qiagen). Genomic DNA was eliminated by both the gDNA eliminator column and on-column incubation with DNase I (79256, Qiagen). Sequencing libraries were constructed and sequenced using TruSeq® Stranded mRNA kit (20020597, Illumina) and NovaSeq 6000.

Bulk RNA-seq analysis

Samples were preprocessed with a standard pipeline that can be viewed at https://github.com/cemalley/Jovanovic_methods. Software used in preprocessing included fastqc 0.11.9, STAR 2.7.8a, trimmomatic 0.39, htseq 3.7.3 (http://www.bioinformatics.babraham.ac.uk/projects/fastqc) (Dobin et al., 2013), (Anders et al., 2015). Analysis was performed in R 4.0.3 (R Core Team 2021 https://www.R-project.org/). Samples were combined with RUVSeq batch correction method RUVg using a set of housekeeping genes (Risso et al., 2014), gene list (Wang et al., 2019).The UCSC Cell Browser cortex development dataset was mined to find unique differentially expressed genes among the radial glia cell subpopulations RGdiv1, oRG, or Pan-RG (https://cells.ucsc.edu/?ds=cortex-dev). DESeq2 was used to merge and normalize samples with the median-of-ratios method (Love et al., 2014). Normalized counts from the resulting R object were row Z-score transformed and scaled before plotting a subset of the DE RG genes, key pluripotency and astrocyte markers in a heatmap using ComplexHeatmap 2.6.2 (Gu et al., 2016). Several public RNA-Seq datasets were obtained from the Sequence Read Archive and merged with the day 30 and day 50 iPSC-astrocyte samples (Figure 4): PRJNA412090 or GSE104232 (Tchieu et al., 2019) (https://www.ncbi.nlm.nih.gov/bioproject/PRJNA412090); PRJNA382448 or GSE97619(Santos et al., 2017) (https://www.ncbi.nlm.nih.gov/bioproject/PRJNA382448); PRJNA383243 or GSE97904(Tcw et al., 2017) (https://www.ncbi.nlm.nih.gov/bioproject/PRJNA383243); and PRJNA297760 or GSE73721(Zhang *et al.*, 2016) (https://www.ncbi.nlm.nih.gov/bioproject/PRJNA297760). Merging was done with the same RUVSeq RUVg method as described previously. Principal component analysis plots were created in R with base function prcomp. Gene set enrichment was performed using the top 100 DE genes per contrast and input to Enrichr, querying the Gene Ontology 2019 or ARCHS4 Tissues databases. Regional marker genes were derived from a list of previously published genes showing significant differential gene expression across eight regions of the developing brains at Carnegie stage 22. (Eze et al., 2021). The ten most-significant genes (adjusted p-value) from each region were used to filter normalized count data from newly

generated time-course RNA-seq for astrocyte differentiation. Clustering of samples was performed with the dendsort R package, gene clustering and heatmap were produced with the pheatmap and viridis R packages (Figure S4).

ATAC-seq and MeDIP-seq analysis

Raw Data. ATAC-seq and MeDIP-seq experiments were performed by Active Motif (Carlsbad, CA, USA) and initial analyses provided included the following: 1. Sequencing and mapping paired-end Illumina sequencing reads to the reference human hg38 genome using BWA; 2. Alignment and peak calling statistics (using MACS2); 3. Generating summary statistics across samples comparisons; 4. Annotation of all intervals (peak regions); 5. Gene-centric rollup of the intervals table; 6. A top table comparing peak region metrics between different samples; 7. A UCSC custom tracks BED file; and 8. A signal map bigwig URL file for viewing in the UCSC viewer.

Modified differential peak analysis. Active Motif included all identified peaks in MACS2. To conservatively assess differential accessibility or methylation, only peaks supported by at least two biological replicates were retained for downstream analysis. DESeq-2 was then run on the filtered peaks (separately for ATAC-seq and MeDIP-seq) using default parameters.

For MeDIP-seq analysis reference genome for human hg38 was generated in BWA, paired-end fastq files aligned to the reference and counts generated using Rsubread with featureCounts (specifying paired-ends). DESeq2 was then used to normalize counts using the “median by ratios” method and used to run differential peak analysis for all pairwise comparisons (iPSC day 0 vs RGCs day 7; iPSC Day 0 vs astrocytes D30 and astrocytes D50; RGC Day 7 vs astrocytes D30 and astrocytes D50).

Overrepresentation analysis. After performing differential peak analysis, peaks were retained if their adjusted p-value was less than 0.05, the peaks ranked by adjusted p-value and overrepresentation analysis was performed using all Gene Ontology (GO) gene sets and Kyoto Encyclopedia of Genes and Genomes (KEGG) 2019 with the R library, clusterProfiler using Benjamini Hochberg correction and an adjusted p-value cut-off of 0.01.

Principal Component Analysis (PCA). For ATAC-seq and MeDIP-seq data, PCA was performed to determine each peak’s variability across samples and genome-wide. The purpose behind performing this analysis was to determine which peak drives the variance across a given gene locus. For some gene loci, there were several

identified ATAC-seq and MeDIP-seq peaks; however, it was not clear which peak might be driving differential accessibility or methylation. To perform this analysis, normalized count data was used in the prcomp function in R to perform PCA. For each gene, the peak with the largest variance was extracted from the PCA. Only peaks within 1,000 base pairs of an annotated gene were included in this analysis (which excludes enhancer elements that are far up-or downstream of a given gene).

The pre-filtered peak per gene with the highest variance was used to build dot plots for a targeted list of genes. All samples and normalized counts were used to calculate the interquartile range (IQR) for each gene (peak), separately. For each gene, peak and sample, the normalized count data was specified by the following criterion: 1. The median of the normalized counts was less than 0.25 quartile: Inaccessible (hypo-methylated); 2. The median of the normalized counts was greater than 0.75 quartile: Hyper-accessible (hyper-methylated); or 3. The median of the normalized counts was between 0.25 and 0.75 quartiles: Mid-accessible (mid-methylated). The above criterion was used to generate the dot plots shown in Figures 5D and 5G.

Single-cell RNA sequencing

Cryopreserved vials of single cell suspensions (1Mio. cells/ml) of hESC-Astrocytes, iCell Astrocytes and iGluta neurons were sent to GENEWIZ for single cell RNA sequencing. Samples were submitted in technical duplicates with a minimum of ≥90% viability post thaw. Additionally, to assist with samples that are submitted with ≤90% viability post thaw, GENEWIZ has implemented a dead cell removal workflow to enhance sample viability.

For single cell RNA-sequencing, 10X Genomics Chromium platform was used. After the library preparations, samples were sequenced on the Illumina HiSeq4000 in a 2x150bp fashion.

Single-cell RNA sequencing data analysis

BCL files produced by the Illumina sequencer were converted to FASTQ files using command mkfastq from theCellRangeranalysis toolkit (10X Genomics, v. 3.1.0,). The FASTQ files were processed with CellRanger count to produce count matrices suitable for analysis in R using package Seurat1(v. 4.0.3).Identification of clusters was performed in Seurat using the Leiden algorithm2(argument “algorithm=4”) at a resolution of 0.4. Pseudotime trajectory analysis was performed using slingshot (Street et al., 2018) and the analysis of the

dynamics of gene expression relative to the previously identified trajectories was performed using tradeSeq (Van den Berge et al., 2020). Integration with external data for the purpose of UMAP visualization was performed using Seurat. Gene set enrichment analysis was performed in R using Enrichr (package “enrichR”). All plots were constructed using ggplot28.The analysis scripts are available at https://github.com/jaro-slamecka/Jovanovic_astrocyte_scRNA-seq.

References

Anders, S., Pyl, P.T., and Huber, W. (2015). HTSeq--a Python framework to work with high-throughput sequencing data. Bioinformatics *31*, 166-169. 10.1093/bioinformatics/btu638.

Dobin, A., Davis, C.A., Schlesinger, F., Drenkow, J., Zaleski, C., Jha, S., Batut, P., Chaisson, M., and Gingeras, T.R. (2013). STAR: ultrafast universal RNA-seq aligner. Bioinformatics *29*, 15-21. 10.1093/bioinformatics/bts635.

Gu, Z., Eils, R., and Schlesner, M. (2016). Complex heatmaps reveal patterns and correlations in multidimensional genomic data. Bioinformatics *32*, 2847-2849. 10.1093/bioinformatics/btw313.

Love, M.I., Huber, W., and Anders, S. (2014). Moderated estimation of fold change and dispersion for RNA-seq data with DESeq2. Genome Biol *15*, 550. 10.1186/s13059-014-0550-8.

Risso, D., Ngai, J., Speed, T.P., and Dudoit, S. (2014). Normalization of RNA-seq data using factor analysis of control genes or samples. Nature Biotechnology *32*, 896-902. 10.1038/nbt.2931.

Tristan, C.A., Ormanoglu, P., Slamecka, J., Malley, C., Chu, P.H., Jovanovic, V.M., Gedik, Y., Jethmalani, Y., Bonney, C., Barnaeva, E., et al. (2021). Robotic high-throughput biomanufacturing and functional differentiation of human pluripotent stem cells. Stem Cell Reports *16*, 3076-3092. 10.1016/j.stemcr.2021.11.004.

Wang, Z., Lyu, Z., Pan, L., Zeng, G., and Randhawa, P. (2019). Defining housekeeping genes suitable for RNA-seq analysis of the human allograft kidney biopsy tissue. BMC Med Genomics *12*, 86. 10.1186/s12920-019-0538-z.